Optimizing Interface Conductivity in Electronics

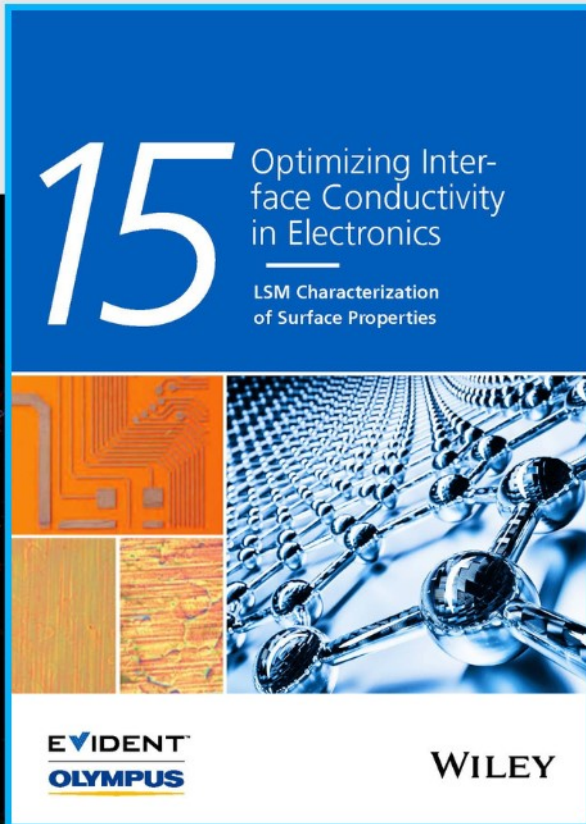

The latest eBook from Advanced Optical Metrology. Download for free.

Surface roughness is a key parameter for judging the performance of a given material's surface quality for its electronic application. A powerful tool to measure surface roughness is 3D laser scanning confocal microscopy (LSM), which will allow you to assess roughness and compare production and finishing methods, and improve these methods based on mathematical models.

Focus on creating high-conductivity electronic devices with minimal power loss using laser scanning microscopy is an effective tool to discern a variety of roughness parameters.

EVIDENT
OLYMPUS

WILEY

ADVANCED ELECTRONIC MATERIALS
Open Access
www.advelectronicmat.de

Check for updates

Controllable and Reproducible Growth of Transition Metal Dichalcogenides by Design of Experiments

Stefan Heiserer, Peter Eder, Cormac Ó Coileáin, Josef Biba, Tanja Stimpel-Lindner, Cian Bartlam, Ulrich Rührmair, and Georg S. Duesberg**

Controllable and reproducible synthesis of 2D materials is crucial for their future applications. Chemical vapor deposition (CVD) promises scalable and high-quality growth of 2D materials. However, to optimize CVD growth, multiple parameters have to be carefully selected. Design of experiments (DoE) is a consistent and versatile tool to optimize all parameters simultaneously in a controlled way. This study exploits DoE statistical approaches to show how the CVD growth of transition metal dichalcogenides (TMDs) can be optimized, using tungsten disulfide as an example. A designed set of 29 different processes is used to cover the entire parameter space. The resulting growth output is characterized in terms of material morphology for factors such as single crystal size and continuous film size. The nonlinear model used to fit the output as a function of input parameters provides crucial insights into the nontrivial CVD process ensuring easy and systematic growth optimization. The predicted processes show successful optimization with respect to both the resulting material and the process stability. This powerful technique can be adapted for different setups and other TMD materials.

1. Introduction

2D materials have gained an enormous interest in academic research due to their unique and tunable electrical and optical properties.[1,2] They have potential for numerous applications in sensing or photonic devices.[3–7] In the large family of semiconducting 2D materials, transition metal dichalcogenides (TMDs) such as tungsten disulfide (WS_2) are promising candidates for future applications due to their outstanding optoelectronic properties.[8,9] Reliable and scalable fabrication of the material is thereby crucial for academic studies and applications.

Chemical vapor deposition (CVD) is largely regarded as the most promising platform for large-scale synthesis of 2D materials including TMDs.[8,10] During the CVD process, gas phase precursors undergo chemical reactions on and near a substrate surface at elevated temperatures, resulting in the deposition of material on the surface.[11] Thereby, a vast parameter space opens up, including different types of precursors, substrates, temperature, gas concentration, flow rate, pressure, process time, and many others.[12,13] Often single process parameters like temperature or carrier gas composition are varied to enhance the output quality.[12] Furthermore, the relationship between growth conditions and the resulting material deposition differs from setup to setup. Thus, reported process parameters cannot be simply copied for other setups and expected to yield the same results. Growth conditions have to be optimized carefully for each setup, and therefore benchmarking of the results is difficult. Regardless all these effort, growth control and reproducibility remains challenging as small changes in the growth conditions can have strong impact on the resulting deposition.[12,14–16]

Design of experiments (DoE) can create a set of experiments where the different input parameters are varied concurrently. This allows one to scan the parameter space within a finite set of growth processes in a more efficient and sophisticated way. Zhang et al. investigated the interaction between different process parameters in CVD growth of TMDs by modeling reported crystal morphologies with respect to corresponding growth settings. However, process settings, outputs, and their relations usually depend on the specific setup used and thus are hardly comparable.[17] Therefore, it is crucial to fix all settings which are not going to be optimized during DoE. Focusing

S. Heiserer, C. Ó Coileáin, J. Biba, T. Stimpel-Lindner, C. Bartlam, G. S. Duesberg
Institute of Physics
Faculty of Electrical Engineering and Information Technology
University of the Bundeswehr Munich and SENS Research Center
Werner-Heisenberg-Weg 39, 85577 Neubiberg, Germany
E-mail: stefan.heiserer@unibw.de; georg.duesberg@unibw.de

P. Eder
Faculty of Physics
LMU Munich
Schellingstraße 4, 80799 München, Germany

U. Rührmair
Institute for Computer Science
LMU Munich
Oettingenstraße 67, 80538 München, Germany

U. Rührmair
Department for Electrical and Computer Engineering
University of Connecticut
371 Fairfield Way, Storrs CT 06269, USA

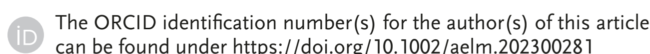

The ORCID identification number(s) for the author(s) of this article can be found under https://doi.org/10.1002/aelm.202300281

© 2023 The Authors. Advanced Electronic Materials published by Wiley-VCH GmbH. This is an open access article under the terms of the Creative Commons Attribution License, which permits use, distribution and reproduction in any medium, provided the original work is properly cited.

DOI: 10.1002/aelm.202300281

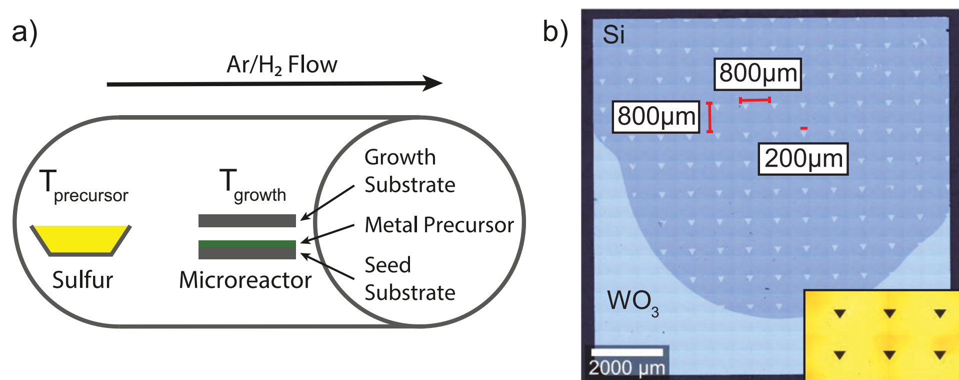

Figure 1. a) Scheme of the CVD setup used for WS_2 growth. b) Patterned WO_3 solid precursor (bright) on Si substrate (dark), including flat continuous part and patterned region (inset).

on 2D materials, optimization using DoE is only reported for graphene CVD synthesis.[18,19] To the best of our knowledge, an experimental and consistent CVD growth optimization for TMDs based on design of experiments has not been reported.

Here we describe a study on the synthesis of WS_2 which demonstrates how DoE statistical approaches can be exploited to optimize CVD growth of TMDs. As different process parameters interact with each other, it is not enough to simply optimize one at a time separately. Five input parameters were varied concurrently to design 29 processes covering the entire parameter space. The corresponding growth results fit a model describing the dependencies of the growth outputs on the process parameters. The established model is used to determine the influential input parameters and to predict the optimized settings needed to enhance growth for various applications. It was successfully tested by directing the growth toward certain crystal qualities like single monolayer crystals or large-area continuous films. In addition, the optimized processes show very good stability and reproducibility. Certainly, the technique presented can easily be applied to other CVD setups, with alternative key parameters, and any TMD material, providing an efficient and systematic method to optimize CVD growth of TMDs.

2. Results and Discussion

2.1. Prestudies: Precursor and Parameter Set

A schematic of setup used for WS_2 growth is shown in **Figure 1**a). It features a microreactor containing a solid state precursor seed and a growth substrate in close contact.[20] The patterned seed substrate shown in Figure 1b) is sputter-coated with oxidized tungsten and serves as metal precursor supply and has patterned and continuous WO_3 areas to prestructure growth. This microreactor design allows the WO_3 precursor to be only supplied locally and avoids potential contamination of the reactor, thus ensuring better run to run comparability. Sulfur, as the chalcogenide precursor, is carried by the Ar/H_2 flow to the growth substrate. The two precursors are at different temperatures $T_{precursor}$ for sulfur and T_{growth} for the microreactor. After preliminary studies, the process parameters and their range were selected according to **Table 1** which defined the extent of the parameter space to be explored. As a fundamental principle for a successful DoE, other

Table 1. Selected input parameters and corresponding value range.

Input parameter	Value range
Growth temperature	800–900 °C
Precursor temperature	100–120 °C
H_2 concentration	10%–50%
Process time	15–45 min
Pressure	2–50 mbar

possible influencing factors were kept consistent and constant as far as possible during experiments.[21] The selection of input parameters heavily depends on the setup and growth method used. Therefore, there is no complete list of input parameters for CVD processes. For example, temperature ramp, type of precursor, or the relative position of the precursor sources with respect to the growth substrate can be optimized.[22,23]

2.2. Design of Experiments

To find optimized and stable growth conditions within the spanned parameter space, a D-optimal design of experiments was used. Optimal designs are commonly used in DoE as they allow versatile choice regarding the number of parameters and their values such that experimental constraints can be accounted for. In a D-optimal design the confidence ellipsoid is minimized to increase the precision of the fit coefficients and the predictions.[24] The designed parameter sets then fractionally cover the entire parameter space within the selected model. Thereby, the vast number of possible combinations within the parameter space was reduced to only 29 processes. As further fundamental principles of DoE, they include repetitions and are in a random order.[21] The details of the performed processes defined within the design can be found Table S1 (Supporting Information).

In the model applied, the output $Y(\mathbf{x})$ depends on linear, quadratic, and interaction terms of the input parameters x_i. In the formula

$$Y(\mathbf{x}) = a_0 + \sum_{i=1}^{p} a_i x_i + \sum_{i=1}^{p} a_{ii} x_i^2 + \sum_{i=1}^{p} \sum_{\substack{j=1 \\ i \neq j}}^{p} a_{ij} x_i x_j \quad (1)$$

 © 2023 The Authors. Advanced Electronic Materials published by Wiley-VCH GmbH

2199160x, 0, Downloaded from https://onlinelibrary.wiley.com/doi/10.1002/aelm.202300281 by Universitat der Bundeswehr Munchen, Wiley Online Library on [31/07/2023]. See the Terms and Conditions (https://onlinelibrary.wiley.com/terms-and-conditions) on Wiley Online Library for rules of use; OA articles are governed by the applicable Creative Commons License

2199160x, 0, Downloaded from https://onlinelibrary.wiley.com/doi/10.1002/aelm.202300281 by Universitat der Bundeswehr Munchen, Wiley Online Library on [31/07/2023]. See the Terms and Conditions (https://onlinelibrary.wiley.com/terms-and-conditions) on Wiley Online Library for rules of use; OA articles are governed by the applicable Creative Commons License

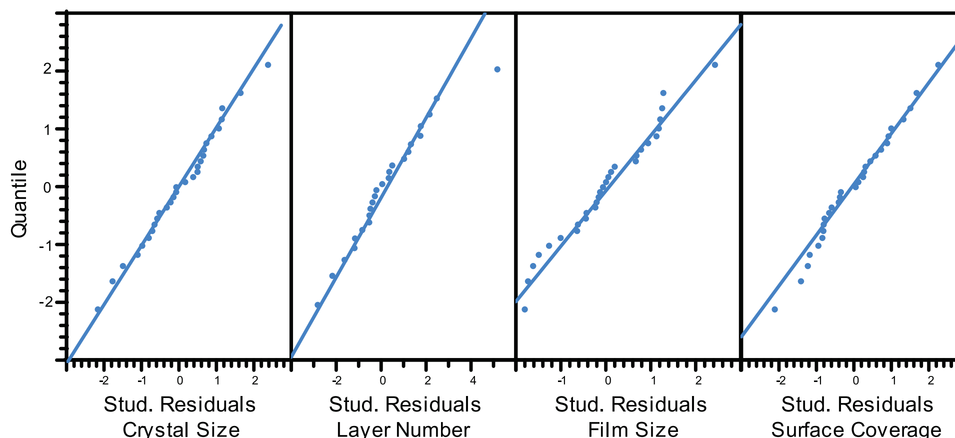

Figure 2. Residual probability plots showing a normal distribution of fit residuals.

a_0 denotes the overall mean response, a_i is the main effect of factor x_i, and a_{ij} is two-way or quadratic interactions between the ith and jth factors.

2.3. Growth Evaluation

After performing the CVD processes, in depth material characterization was performed using Raman spectroscopy, atomic force microscopy (AFM), and optical microscopy (Figure S1, Supporting Information). To fit the selected model, measurable outputs have to be defined. Therefore, the characterization results were combined to derive a consistent and efficient all-optical evaluation routine which takes four output parameters into account: *surface coverage* describes the percentage of growth-covered substrate. *Film size* denotes the side length of the biggest square area with continuously interconnected growth. *Film thickness* is the mean layer number within this area and *single crystal size* the side length of the largest monocrystalline structure on the sample, see the experimental section for more details. The output values averaged over two samples per run are summarized in Table S1 (Supporting Information). Notably, while this data was acquired manually, the output evaluation could be made more efficient using machine learning.[25,26] The measured data was then imported into Cornerstone 7.3 from CamLine for modeling and further evaluation.

2.4. Modeling

Prior to evaluating the impact of different growth parameter combinations, a Box–Cox transformation was applied to all responses in the regression model, including logarithmic and power transformations. Evaluating the Box–Cox diagrams (see Figure S2 in the Supporting Information), the transformations log(crystal size), log(film size), and sqrt(surface coverage) stabilize the variance and produce a better normal distributed fit than the untransformed responses.[27] Layer number remained untransformed for the following evaluation.

Using Equation (1), a fitted model was derived where insignificant terms are excluded.

Table S2 (Supporting Information) shows the coefficients for each model as well as their significance values. The adjusted R-square values for the fits of surface coverage, film size, thickness, and single crystal size are 0.845, 0.913, 0.804, and 0.83, respectively. This indicates already a reliable data set and a correctly chosen model. Moreover, a proper residual analysis was made to ensure trustworthy data interpretation. **Figure 2** shows the residual probability plots for all responses where residuals are plotted against theoretical values of normal probability distribution. Besides one obvious outlier, the residuals stay well within the 3σ range and follow the straight line of normal distribution which is desirable for confidence and significance calculations. Furthermore this confirms that the model chosen is suitable and reliable conclusions and predictions can be made from it.[27]

Figure 3 shows the adjusted response graph which illustrates the relationship between each process parameter and the different output variables. As the impact of the other input parameter is averaged out for each single plot, the graph helps provide a fundamental understanding how different process parameters influence CVD growth. In general, the surface coverage and film size exhibit similar trends. For example, both output values increase with increasing growth temperature until a plateau is reached. Single crystal size follows a similar trend with growth temperature. In contrast, the film thickness decreases at the same time, suggesting lateral growth is preferred at higher temperatures, which is often desired.[28,29] The process pressure has the greatest influence on film thickness and surface coverage shows a maximum at around 25 mbar, but it has almost no influence on film size and single crystal size. Another input parameter H_2 concentration has a significant impact only on film thickness as it increases for both, high and low concentrations. Significantly, process time has no major effect on any of the responses. This finding was confirmed by a test process with a much longer process time of 90 min, which showed no significant change in output parameters and may be attributed to a simultaneous and self-limiting etch effect due to hydrogen in the carrier gas and limited metal precursor.[30,31] The influence of precursor temperature seems to have the most complex trends as it depends heavily on the setting of other parameters. For example, there is a strong interaction between the precursor temperature and both the growth temperature and pressure (see Figure S3 in the

© 2023 The Authors. Advanced Electronic Materials published by Wiley-VCH GmbH

2199160x, 0, Downloaded from https://onlinelibrary.wiley.com/doi/10.1002/aelm.202300281 by Universitat der Bundeswehr Munchen, Wiley Online Library on [31/07/2023]. See the Terms and Conditions (https://onlinelibrary.wiley.com/terms-and-conditions) on Wiley Online Library for rules of use; OA articles are governed by the applicable Creative Commons License

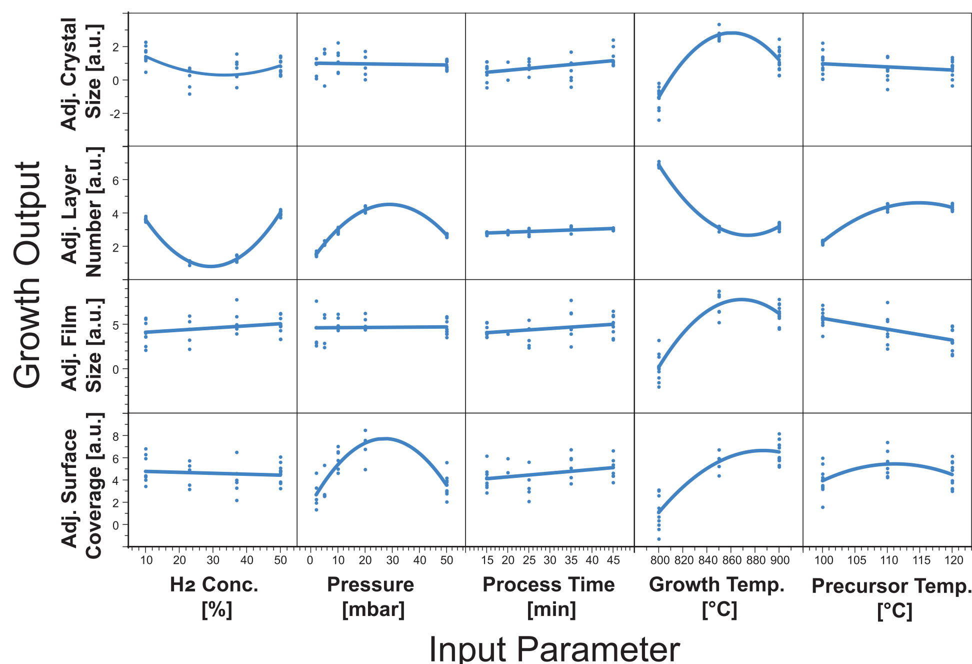

Figure 3. Adjusted response graph for crystal size, layer number, film size, and surface coverage: The influence of each process parameter is shown in the corresponding box. The impact of the remaining input parameters is averaged out.

Supporting Information). The former can be related to maintaining the necessary ratio between metal and sulfur precursor during growth. The latter one confirms increased sulfur evaporation rate at lower pressure.[17]

2.5. Successful Prediction and Growth Control

To achieve high-quality materials for the desired applications, process parameter sets can be predicted to optimize the material with respect to certain aims. These aims can be single or a combination of optimized output values. In our study, we show two examples of possible optimization scenarios: The first aim is single monolayer crystals where crystal size is maximized and layer number minimized at the same time. The second aim is to get samples with high yield of continuous material which is often desired for electrical device applications. Thereby, the two output parameters, film size and surface coverage, are maximized. The optimized process parameters shown in **Table 2** are derived from the fit model to optimize the aim of large single monolayer crystals and or large-area continuous films, respectively. As predicted by the model, the processes using the optimized parameters resulted in enhanced output values. Table 2 compares the values for each objective before and after optimization starting from the best processes found by trial and error over 20 different processes. All values markedly increased, showing controlled growth and successful optimization.

2.6. Optimized Material Quality and Process Stability

To confirm the consistent high quality of the grown material, the optimized processes were performed multiple times. The resulting growth was characterized using Raman and photoluminescence (PL) spectroscopy (see **Figure 4**). In the scenario where the growth was optimized to produce a continuous monolayer film, there is additional bilayer growth which can be seen in optical contrast as well as in PL intensity. Furthermore, the grain boundaries of underlying monolayer film show a decreased signal in the PL intensity map (Figure 4c)). Figure 4d shows an optical micrograph of the sample optimized for single crystals featuring monolayer crystals. The PL map of a 23 µm monolayer single crystal

Table 2. Process parameters for optimized processes toward large monolayer crystals and continuous film.

Aim	Single monolayer crystals	Large film size
Optimized parameters: H_2 conc., pressure, process time, growth temp., precursor temp.	25%, 2 mbar, 40 min, 870, 115 °C	30%, 26 mbar, 30 min, 850, 110 °C
Average value before → after DoE percentage change	8 µm → 19 µm **+137%**	120 µm → 950 µm **+690%**
Standard deviation before → after DoE percentage change	48% → 34% **−29%**	67% → 27% **−59%**

Optimization led to significantly higher output values and lower interprocess standard deviations in both scenarios.

© 2023 The Authors. Advanced Electronic Materials published by Wiley-VCH GmbH

2199160x, 0, Downloaded from https://onlinelibrary.wiley.com/doi/10.1002/aelm.202300281 by Universitat der Bundeswehr Munchen, Wiley Online Library on [31/07/2023]. See the Terms and Conditions (https://onlinelibrary.wiley.com/terms-and-conditions) on Wiley Online Library for rules of use; OA articles are governed by the applicable Creative Commons License

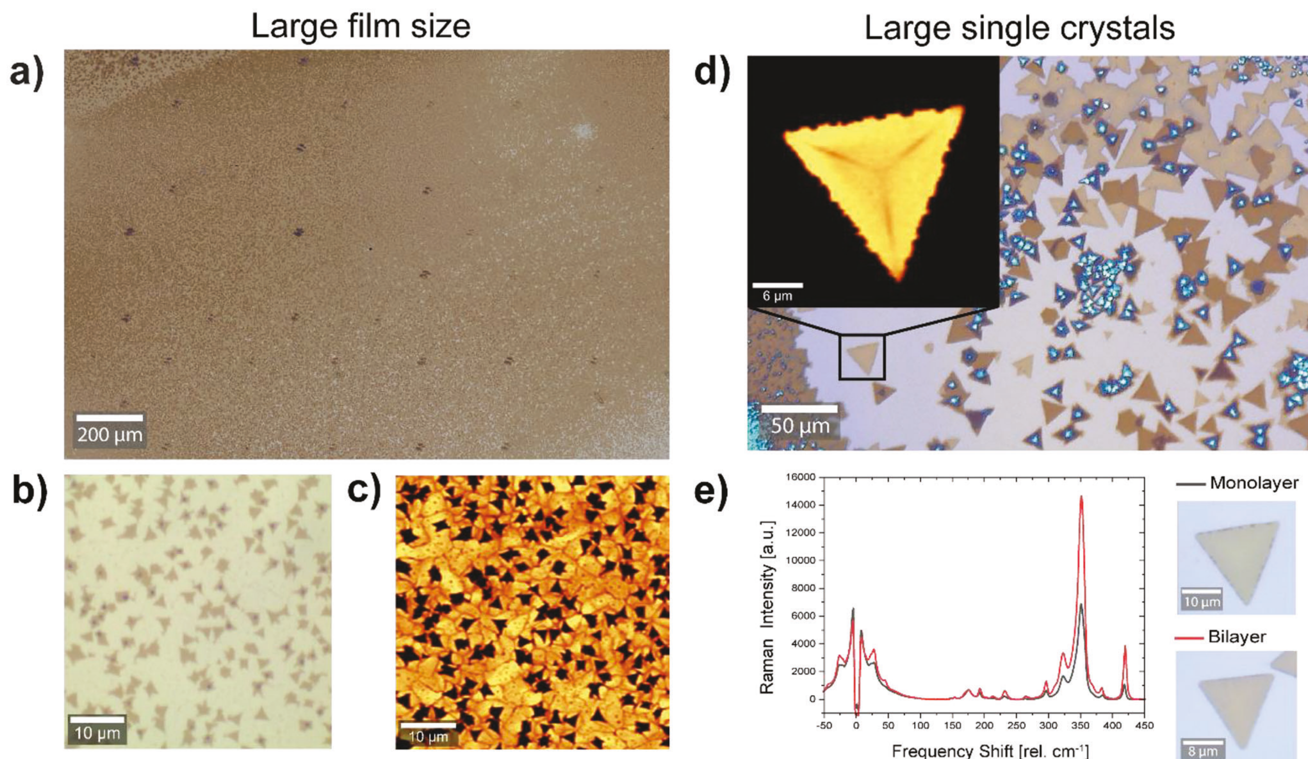

Figure 4. a,b) Optical images of a continuous monolayer film with additional crystalline bilayer regions. c) PL intensity map of WS_2 continuous film showing suppressed intensity along grain boundaries and in bilayer regions. d) Single monolayer (light brown) and bilayer (dark brown) crystals of WS_2. PL intensity map of a 23 µm flake (inset). e) Raman spectra and corresponding optical micrographs of monolayer and bilayer WS_2 single crystals.

(inset of Figure 4d) exhibits a slight intensity decrease along its symmetry axis which is often seen in CVD crystals and can be attributed to tungsten vacancies.[32–34]

As shown in Table 2 not only did the desired output values increase, but moreover the interprocess fluctuations in the outputs, using the same recipe, drastically decreased to values of 34% and 27% standard deviation for the single crystal and film process, respectively. This confirms unique process stability and reproducibility of the CVD-grown material.

3. Conclusions

In summary, CVD growth of WS_2 was optimized by tuning the process parameters using DoE. The output was modeled with regards to surface coverage, film size, layer number, and crystal size to develop an understanding of the basic underlying growth kinetics. Furthermore, the model successfully provided predictions of parameter sets for different application scenarios including single monolayer crystals and large continuous films. For all of them, the predicted processes show optimized results and moreover enhanced stability due to drastically decreased interprocess fluctuations. Our technique offers a straightforward and coherent route to get controllable and stable growth which can be tuned for the desired application. Moreover, the technique is not limited to morphology evaluation. Electrical characteristics could be used as an output parameter to further refine and direct the growth or properties of the materials. We believe the approach can easily be adapted to broader application areas including different TMD materials and other CVD methods with different growth parameters. Thereby, mapping the scope of the parameter space through DoE may offer a route to realistically compare the materials produced in different CVD setups.

4. Experimental Section

Precursor Synthesis and CVD Growth: WO_3 seed substrates were prepared by patterned deposition of 10–20 nm of tungsten on silicon substrates and subsequent oxidation under low pressure O_2/Ar atmosphere at 550 °C for 10 h. Growth substrates (Si with 90/300 nm thermal SiO_2) were cleaned in acetone and IPA in an ultrasonic bath and placed face down on top of the WO_3 substrates. The microreactor design allows the WO_3 precursor to be only supplied locally and avoids potential contamination of the reactor with excess materials, thus ensuring better run to run comparability. The WO_3 source substrates were replaced for each experiment with the same quantity and configuration of WO_3. The samples were placed in a ceramic boat within the hot zone of the quartz tube furnace. A second movable furnace was used to heat the sulfur powder placed within a boat upstream the tube. When the main furnace reached the set process temperature, the sulfur furnace was moved toward the main furnace heating the sulfur to the set precursor temperature. At the same time the process time started and 20 sccm of H_2 was added to the carrier gas. The argon flow was thereby adjusted with respect to the set H_2 concentration. After the process the H_2 flow was stopped and precursor supply rapidly stopped by moving the sulfur furnace away from the precursor source.

Material Characterization: Photoluminescence and Raman spectra were recorded using a Witec alpha 300 R under 532 nm laser excitation. AFM was performed using a Jupiter XR Asylum Research from Oxford Instruments in tapping mode. For the growth output evaluation for the DoE

 © 2023 The Authors. Advanced Electronic Materials published by Wiley-VCH GmbH

an all-optical method was developed using the optical mode of the Raman microscope with different magnifications. The layer number of the crystals was clearly identified by optical contrast.

Data Analysis: For design of experiments the software Cornerstone 7.3 from CamLine GmbH was used. Input factors and responses were defined relating to the process parameters and measured output, respectively. A model was selected including linear, quadratic, and interaction terms. The process runs were then chosen using a D-optimal design.

Supporting Information

Supporting Information is available from the Wiley Online Library or from the author.

Acknowledgements

This project was funded by dtec.bw—Digitalization and Technology Research Center of the Bundeswehr for support (project VITAL-SENSE). dtec.bw is funded via the German Recovery and Resilience Plan by the European Union (NextGenerationEU). Further, this project was supported by the European Union's Horizon 2020 Research and Innovation Program under grant agreement no. 881603 (Graphene Flagship Core 3) and the European Union's HORIZON-EIC-2021 under the project no. 101046693 (SSLiP). The authors also thank the German Federal Ministry for Education and Research (BMBF) for support under project 16ES1121 NobelNEMS. U.R. acknowledges support by the AFOSR Grant No. FA9550-21-1-0039.

Open access funding enabled and organized by Projekt DEAL.

Conflict of Interest

The authors declare no conflict of interest.

Data Availability Statement

The data that support the findings of this study are available from the corresponding author upon reasonable request.

Keywords

2D materials, chemical vapor deposition, design of experiments, growth optimization, synthesis, transition metal dichalcogenides, tungsten disulfide

Received: April 29, 2023
Revised: June 15, 2023
Published online:

[1] Q. H. Wang, K. Kalantar-Zadeh, A. Kis, J. N. Coleman, M. S. Strano, *Nat. Nanotechnol.* **2012**, *7*, 699.
[2] R. Tilmann, C. Weiß, C. P. Cullen, L. Peters, O. Hartwig, L. Höltgen, T. Stimpel-Lindner, K. C. Knirsch, N. McEvoy, A. Hirsch, G. S. Duesberg, *Adv. Electron. Mater.* **2021**, *7*, 2000564.
[3] S. Parhizkar, M. Prechtl, A. L. Giesecke, S. Suckow, S. Wahl, S. Lukas, O. Hartwig, N. Negm, A. Quellmalz, K. Gylfason, D. Schall, M. Wuttig, G. S. Duesberg, M. C. Lemme, *ACS Photonics* **2022**, *9*, 859.
[4] K. Lee, B. M. Szydłowska, O. Hartwig, K. Synnatschke, B. Tywoniuk, T. Hartman, T. Tomašević-Ilić, C. P. Gabbett, J. N. Coleman, Z. Sofer, M. Spasenović, C. Backes, G. S. Duesberg, *J. Mater. Chem. C* **2023**, *11*, 593.
[5] R. Gatensby, T. Hallam, K. Lee, N. McEvoy, G. S. Duesberg, *Solid-State Electron.* **2016**, *125*, 39.
[6] L. von Lüders, R. Tilmann, K. Lee, C. Bartlam, T. Nevanen, K. Iljin, K. C. Knirsch, A. Hirsch, G. S. Duesberg, *Angew. Chem., Int. Ed.* **2023**, *62*, e202219024.
[7] K. Lee, R. Gatensby, N. McEvoy, T. Hallam, G. S. Duesberg, *Adv. Mater.* **2013**, *25*, 6699.
[8] C. Lan, C. Li, J. C. Ho, Y. Liu, *Adv. Electron. Mater.* **2021**, *7*, 2000688.
[9] C. Cong, J. Shang, Y. Wang, T. Yu, *Adv. Opt. Mater.* **2018**, *6*, 1700767.
[10] H. F. Liu, S. L. Wong, D. Z. Chi, *Chem. Vap. Deposition* **2015**, *21*, 241.
[11] J. R. Creighton, P. Ho, *Introduction to Chemical Vapor Deposition (CVD)*, ASM International, Materials Park, OH **2001**.
[12] K. M. McCreary, A. T. Hanbicki, G. G. Jernigan, J. C. Culbertson, B. T. Jonker, *Sci. Rep.* **2016**, *6*, 19159.
[13] D. Zhou, H. Shu, C. Hu, L. Jiang, P. Liang, X. Chen, *Cryst. Growth Des.* **2018**, *18*, 1012.
[14] S. Kumar, N. McEvoy, H.-Y. Kim, K. Lee, N. Peltekis, E. Rezvani, H. Nolan, A. Weidlich, R. Daly, G. S. Duesberg, *Phys. Status Solidi B* **2011**, *248*, 2604.
[15] C. Wirtz, K. Lee, T. Hallam, G. S. Duesberg, *Chem. Phys. Lett.* **2014**, *595–596*, 192.
[16] J. Lin, S. Monaghan, N. Sakhuja, F. Gity, R. K. Jha, E. M. Coleman, J. Connolly, C. P. Cullen, L. A. Walsh, T. Mannarino, M. Schmidt, B. Sheehan, G. S. Duesberg, N. McEvoy, N. Bhat, P. K. Hurley, I. M. Povey, S. Bhattacharjee, *2D Mater.* **2020**, *8*, 025008.
[17] J. Zhang, F. Wang, V. B. Shenoy, M. Tang, J. Lou, *Mater. Today* **2020**, *40*, 132.
[18] R. Shanmugam, M. Rangarajan, S. Devanathan, V. G. Sathe, R. Senthilkumar, N. K. Kothurkar, *Mater. Res. Express* **2016**, *3*, 125601.
[19] R. Papon, C. Pierlot, S. Sharma, S. M. Shinde, G. Kalita, M. Tanemura, *Phys. Status Solidi B* **2017**, *254*, 1600629.
[20] M. O'Brien, N. McEvoy, T. Hallam, H.-Y. Kim, N. C. Berner, D. Hanlon, K. Lee, J. N. Coleman, G. S. Duesberg, *Sci. Rep.* **2014**, *4*, 7374.
[21] J. K. Telford, *Johns Hopkins APL Technical Digest* **2007**, *27*, 224.
[22] Q. Wu, H. Nong, R. Zheng, R. Zhang, J. Wang, L. Yang, B. Liu, *Angew. Chem., Int. Ed.* **2023**, e202301501.
[23] Q. Wu, Y. Luo, R. Xie, H. Nong, Z. Cai, L. Tang, J. Tan, S. Feng, S. Zhao, Q. Yu, J. Lin, G. Chai, B. Liu, *Small* **2022**, *18*, 2201051.
[24] P. F. Aguiar, B. Bourguignon, M. S. Khots, D. L. Massart, R. Phan-Than-Luu, *Chemom. Intell. Lab. Syst.* **1995**, *30*, 199.
[25] P. A. Larsen, J. B. Rawlings, N. J. Ferrier, *Chem. Eng. Sci.* **2007**, *62*, 1430.
[26] A. Ziletti, D. Kumar, M. Scheffler, L. M. Ghiringhelli, *Nat. Commun.* **2018**, *9*, 2775.
[27] T. Wember, Technische Statistik und statistische Versuchsplanung. Einführung in statistische Methoden mit Anwendungsschwerpunkt in der Analyse technischer Daten, Version 8.5.
[28] J. Chen, K. Shao, W. Yang, W. Tang, J. Zhou, Q. He, Y. Wu, C. Zhang, X. Li, X. Yang, Z. Wu, J. Kang, *ACS Appl. Mater. Interfaces* **2019**, *11*, 19381.
[29] Q. Xiang, X. Yue, Y. Wang, B. Du, J. Chen, S. Zhang, G. Li, C. Cong, T. Yu, Q. Li, Y. Jin, *Nano Res.* **2021**, *14*, 4314.
[30] X. Xin, Y. Zhang, J. Chen, M.-L. Chen, W. Xin, M. Ding, Y. Bao, W. Liu, H. Xu, Y. Liu, *Mater. Horiz.* **2022**, *9*, 2416.
[31] X. Zhang, H. Nan, S. Xiao, X. Wan, X. Gu, A. Du, Z. Ni, K. K. Ostrikov, *Nat. Commun.* **2019**, *10*, 598.
[32] B. G. Jeong, C. Lee, S. H. Kim, S. J. Yun, D. H. Kim, J. Lee, D. Lee, K. K. Kim, S. C. Lim, M. S. Jeong, *J. Phys. Chem. C* **2022**, *126*, 7177.
[33] M. R. Rosenberger, H.-J. Chuang, K. M. McCreary, C. H. Li, B. T. Jonker, *ACS Nano* **2018**, *12*, 1793.
[34] B. L. T. Rosa, K. Fujisawa, J. C. C. Santos, T. Zhang, M. J. S. Matos, F. B. Sousa, T. C. Barbosa, L. Lafeta, S. L. L. M. Ramos, B. R. Carvalho, H. Chacham, B. R. A. Neves, M. Terrones, L. M. Malard, *Phys. Rev. B* **2022**, *106*.

© 2023 The Authors. Advanced Electronic Materials published by Wiley-VCH GmbH

2199160x, 0, Downloaded from https://onlinelibrary.wiley.com/doi/10.1002/aelm.202300281 by Universitat der Bundeswehr Munchen, Wiley Online Library on [31/07/2023]. See the Terms and Conditions (https://onlinelibrary.wiley.com/terms-and-conditions) on Wiley Online Library for rules of use; OA articles are governed by the applicable Creative Commons License